

Multi-Lead ECG Classification via an Information-Based Attention Convolutional Neural Network

Hao Tung, Chao Zheng, Xinsheng Mao, and Dahong Qian,

Abstract—Objective: A novel structure based on channel-wise attention mechanism is presented in this paper. Embedding with the proposed structure, an efficient classification model that accepts multi-lead electrocardiogram (ECG) as input is constructed. **Methods:** One-dimensional convolutional neural networks (CNN) have proven to be effective in pervasive classification tasks, enabling the automatic extraction of features while classifying targets. We implement the Residual connection and design a structure which can learn the weights from the information contained in different channels in the input feature map during the training process. An indicator named mean square deviation is introduced to monitor the performance of a particular model segment in the classification task on the two out of the five ECG classes. The data in the MIT-BIH arrhythmia database is used and a series of control experiments is conducted. **Results:** Utilizing both leads of the ECG signals as input to the neural network classifier can achieve better classification results than those from using single channel inputs in different application scenarios. Models embedded with the channel-wise attention structure always achieve better scores on sensitivity and precision than the plain Resnet models. The proposed model exceeds the performance of most of the state-of-the-art models in ventricular ectopic beats (VEB) classification, and achieves competitive scores for supraventricular ectopic beats (SVEB). **Conclusion:** Adopting more lead ECG signals as input can increase the dimensions of the input feature maps, helping to improve both the performance and generalization of the network model. **Significance:** Due to its end-to-end characteristics, and the extensible intrinsic for multi-lead heart diseases diagnosing, the proposed model can be used for the real-time ECG tracking of ECG waveforms for Holter or wearable devices.

Index Terms—Attention models, Convolutional neural network (CNN), ECG classification, Arrhythmia.

I. INTRODUCTION

IN 1903, Willem Einthoven recorded the first clear human ECG, opening a new era of clinical applications of ECG. Over the past 100 years, thousands of ECG workers, cardiologists and biomedical engineers have laid the foundation, exploration and innovation to make world-famous contributions to the protection of human health and the saving of countless lives. An electrocardiogram is a simple, inexpensive, easy-to-follow observation and an important clinical support program that contains a wealth of information describing the

state of cardiac electrophysiology. Electrocardiography is of great value in the diagnosis of abnormal origins of cardiac activation and conduction abnormalities. Arrhythmia describes a group of important diseases among cardiovascular diseases. It can occur alone or in conjunction with other cardiovascular diseases. Many rapid and slow arrhythmias can be diagnosed by ECG, such as various premature beats, supraventricular atrial fibrillation, atrial flutter, atrial fibrillation and so on.

However, only experienced cardiologists can easily distinguish between abnormal heartbeats and normal sinus rhythms by observing an electrocardiogram, and it is unlikely that patients with arrhythmia will be monitored by a professional doctor in real time. Standard 12-lead ECGs that are very effective for the diagnosis of multiple heart diseases are often not a means of long-term detection. Although an improved lead configuration facilitates the patient's basic activities (changing the limb lead to the chest side), the signal changes significantly due to changes in the position of the measuring electrode, and some related studies have shown that this placement changes the electrocardiogram's clinical specificity [1]. Furthermore, the ECG features of certain arrhythmias are subject-specific and closely related to the physical state and the physiological factors of the subject [2] [3]. Differences in ECG measuring instruments and various measurement environments both pose challenges to the task of automatically detecting ECG using computers.

Early researchers used the “two-stage” idea of feature extraction and classification to do much research work on the diagnosis of arrhythmia: using structural and statistical knowledge of the ECG signal classified by a hidden Markov model [4], constructing filter banks that decomposes the ECG into sub-bands with uniform frequency bandwidths [5], classifying the ECG with its morphological information and timing information by a feed-forward multilayer perceptron neural network [6], developing a statistical model towards ECG morphology with intervals features [7], extracting ECG's higher order statistics and Hermite coefficients classified by a support vector machine (SVM)[3], developing morphological and temporal features classified by a multilayer perceptron [8], applying multi-resolution wavelet transform features with SVM classifier [9]. However, as mentioned in [10], due to the complex and variable application scenarios of the algorithm, the generalization performance of the two-stage algorithms remains to be proven.

With the exaltation of computer functions and the rapid development of neural network technology, computer-aided ECG analysis has developed by leaps and bounds. However, most works related to the classification of arrhythmia are

H. Tung is with the Institutes of Biomedical Engineering, Shanghai Jiaotong university, China, (e-mail: twistfatezz@sjtu.edu.cn).

Chao Zheng and Xinsheng Mao are with Shukun (Beijing) Network Technology Co.,Ltd.

D.H. Qian is with the Institutes of Medical Robotics, Shanghai Jiaotong University, China, (e-mail: dahong.qian@sjtu.edu.cn)

Key research and development project in Zhejiang Province, China: “Wearing human body physiological parameter monitoring technology and equipment research and development – 5-parameter wearable device and cloud platform based on body area network”, Grant No. 2017C03029.

based on single-lead ECG signals. Many studies such as [10], [11] and [12] chose to use the upper lead in the MIT-BIH arrhythmia database (mitdb) but not the lower lead, in which the ventricular ectopic beats (VEB) and supraventricular ectopic beats (SVEB) signals are more conspicuous. Other studies such as [13], [14], [15] and [16] only use the lead II ECG signal in their chosen database. As far back as 1989, the American Heart Association suggested that monitors should be able to analyze three or more leads [17]. According to [18], multi-lead ECG analysis is an effective method to improve the detection accuracy and reduce false positive alarms. Yan et al. [19] experimentally proved that the use of multi-lead data results in more reliability and higher accuracy. However, relatively few studies have used multi-lead ECG data. In the process of handling multi-lead ECG issues, most works combined the feature vectors by direct concatenation [20] and in some cases the final classification report is derived by multi-lead results fusion [18], [19]. Chazal et al. [20], directly connected the feature vectors obtained by sampling each lead of the ECG signal in the feature fusion step. La et al. [21] derive the final prediction by training a set of weighting coefficients for the result produced by each lead. The concatenate approach is equivalent to treating the features extracted by different leads as if they are from the “same lead”. Since the ECG signals are derived from different leads, the positions of the different lead signal acquisition electrodes are different, and they do not have intrinsic homology. The fusion of eigenvectors has no “lead difference”, and the direct splicing of features is debatable. Automatic feature extraction and feature fusion through neural networks are necessary.

It should be noted that some arrhythmias have strong specificities. The QRS waveform characteristics of the left bundle branch block are related to the age of the subject and have lead specificity. Most types of arrhythmia diseases such as right bundle branch block and premature beats also conform to the above argument that totally different morphological characteristics appear on different leads. Indeed, the 12-lead ECG measurement is cumbersome, and it is practical to use fewer leads to diagnose some of the arrhythmias. The Precise diagnosis of arrhythmias or more complex heart diseases, as well as the localization of lesions, requires a joint analysis of multiple leads. Developing a model that automatically fuses different lead features will increase the upper limit of the ECG analysis algorithm. The greater the number of ECG leads analyzed, the better is the interpretability and reliability of the “electrophysiological portrait” of the subject. Therefore, computer-aided multi-lead diagnosis has important research significance and clinical value.

Considering the multiple factors above, the mitdb was selected as the research basis of this study. We establish a weight calibration structure called the information-based squeeze and excitation block (ISE-block) for different feature channels in the neural network model to enhance the neural network model’s ability to extract features and the ability to achieve feature fusion based on multi-channel ECG input, which can improve the detection and diagnosis level of the CNN model in the ECG signal classification and recognition task. We adopt the end-to-end convolutional neural network

model as the backbone of our ISE structure. A set of control experiments is conducted to prove that the application of two leads for ECG classification is more effective. For the ISE structure proposed in this study, an ablation study is implemented to verify the benefits of the structure’s feature channel recalibration function on the ECG classification task. We introduce patient-specific scheme for the comparison with some state-of-the-art models, in which an individual attention model is trained for each patient.

The rest of this article is organized as follows. Section II outlines the ECG dataset used in this study, as well as the corresponding dataset preprocessing methods for the control trials, including descriptions of the lead configuration, ECG data processing and dataset partitioning. Several network models for the ablation experiments are presented in Section III, and the structure of the proposed ISE-block, together with corresponding basic mathematical expressions is described. In Section IV, we introduce the objective function, the algorithm optimizer, the evaluation index of the proposed model, and the framework used for programming. The results of all the control experiments performed in this study are presented in Section V with careful analysis. Section VI summarizes the experimental results and provides a profound discussion of the principles and performance of the proposed structure. Section VII summarizes the work of the entire study. The theoretical basis for supporting ISE-block design is neatly expressed in Appendix A.

II. METHODOLOGY

A. Database

The mitdb [2] is used in this study. The benchmark database was established by the Beth-Israel Hospital in Boston and the MIT Lab. It is the first dataset to contain standard test materials that are widely used to evaluate the performance of arrhythmia detectors, and is the only one indicated by the Association for the Advancement of Medical Instrumentation (AAMI) standard that contemplates all 5 of the superclasses for arrhythmias [22]. This database has been widely used in some remarkable studies [7], [10], [23], [24], [25], and [26]. The database contains 48 thirty minute-long two-channel Holter recordings obtained from 47 subjects in the BIH Arrhythmia Laboratory from 1975 to 1979. Twenty-three of the records are randomly selected from a dataset containing 4000 twenty-four-hour dynamic ECG records, and the other 25 records are selected from the same dataset to contain some uncommon but clinically significant cases. The ECG data of each channel in the database are digitized at a specification of 360 Hz sampling points per second. Each beat is labeled by two or more cardiologists for each record in the database, with the R-wave peak or local extrema of the beat noted.

B. ECG Signal Preprocessing

The mitdb contains more than 30 kinds of annotations, including beat-level annotations, wave-level annotations, and signal-related annotations, in which a variety of arrhythmia signals are attentively annotated. Although various types of cardiac arrhythmias exist, AAMI [27] recommends that only

some types should be detected by equipment or algorithms [22]. According to the AAMI recommendations, there are 17 recommended arrhythmia categories that are classified into 5 superclasses. The following mappings of categories are based on [28]: N: Normal beat (1), Left bundle branch block beat (2), Right bundle branch block beat (3), and Left or right bundle branch block (25); S: Aberrated atrial premature beat (4), Nodal (junctional) premature beat (7), Atrial premature contraction (8), Premature or ectopic supraventricular beat (9), Nodal (junctional) escape beat(11), Atrial escape beat (34), and Supraventricular escape beat (35); V: Premature ventricular contraction (5), and Ventricular escape beat (10); F: Fusion of ventricular and normal beat (6); and Q: Paced beat (12), Unclassifiable beat (13), and Fusion of paced and normal beat (38). All data used in the experiments in this study were processed according to the classification suggested by the practice recommended by AAMI ECAR-1987 [27].

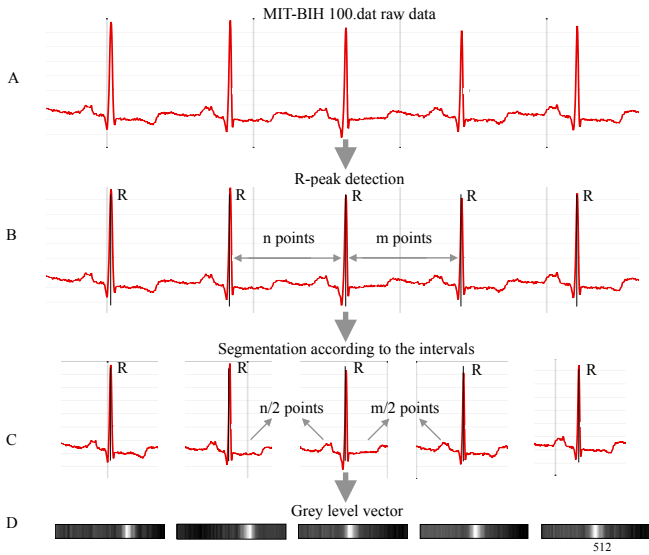


Fig. 1. Data preprocessing pipeline using heartbeats in the mitdb record 100.

1) *Lead Configuration*: In most records of the mitdb, the upper signal is a modified limb lead II (MLII), obtained by placing the electrodes on the chest. The lower signal is usually a modified lead V1 (occasionally V2 or V5, and in one instance, V4), and as for the upper signal, the electrodes are also placed on the chest [29] [30]. According to the website located at <https://www.physionet.org>, normal QRS complexes are usually prominent in the upper signal, while the normal beats are frequently difficult to discern in the lower signal, although ectopic beats (SVEB and VEB) will often be more prominent. Considering the above factors, three lead configurations are adopted for the control experiments: MLII, V1, and MLII together with V1.

2) *Record Excluded*: In records 102 and 104, it was not possible to use the modified lead II because of surgical dressings on the patients. Four of the 48 records (102, 104, 107, and 217) include paced beats [29] [30], so we exclude them in our experiments. Since we need to use two lead signals, we must ensure the consistency of the leads in all the samples—the first lead must be a modified lead II and the second lead is V1. Records 100, 103, 114, 117, 123 and 124

are excluded because their second signal was not acquired via lead V1. The remaining 38 records are used as the dataset for the following experiments.

3) *Data Refactoring Pipeline*: Fig. 1 shows the pipeline of the ECG data preprocessing procedures. We split the ECG signal in a similar way to that used in [11], but after the segmentation, the alignment step is not used. Part A in Fig. 1 shows the original ECG signal in the mitdb converted from the format 212 to the analog electrical signal¹. R-peak detection is shown in part B in Fig. 1. Many advanced R-peak detection methods such as [31], [32], and [33] can be used for the mitdb. We directly split the database according to its original annotation. The time series of ECG signals are separated according to the sampling rate and the locations of the R-peaks, as shown in part C in Fig. 1. Specifically, the signal is cut at beat by beat at the points, which is half of the number the sampling points away from two adjacent R peaks, to produces dynamically segmented heartbeats. The number of sampling points for one segmented beat is computed as follows:

$$N_{R_j} = I_{R_j} + I_{R_{j+1}} + 1 \quad (1)$$

R_j is the j -th R peak, I_{R_j} is the number of sampling points of the interval of R_j and R_{j-1} , and N_{R_j} is the number of sampling points of j -th ECG waveform centered on the j -th R-peak. Segmented ECG heartbeats are transformed into 1D vectors, as shown in part D in Fig. 1. We implement necessary filtering of the signal to remove high-frequency noise and baseline drift and the normalization of the analog voltage values in each beat is adopted to accelerate the training convergence process. To best preserve the morphological features of the heartbeat samples, while taking into account the model's algorithm and implementation framework, statistical analysis is used to overview the length information of the samples in the training set and the cubic spline interpolation method is used to supplement the heartbeats in a batch to the same length of 512 points. Some training heartbeats segmented has irregular length, we remove them for better performance of our algorithm. Random downsampling is used for the samples above 512 points. The way data are preprocessed, especially for signals with timing characteristics, is of great importance, and inappropriate processing will result in classification mess. For premature beat waveforms, padding zeros in front of the waveform may cause serious characteristic changes, and it can be the reason why many proposed algorithms are confused in distinguishing between N and S classes. The ECG signals of the two leads in the mitdb used for models that accept dual-lead signal inputs are reconstructed in the manner shown in Fig. 2.

4) *Separate Training Test*: According to the work of [34], there are two ways to divide the dataset, which are called “class-oriented” and “subject-oriented” methods. We implemented the subject-oriented data partitioning method to conduct a series of control experiments and the patient-specific scheme is taken into consideration. We divide 38 records into

¹More details about format 212 can be found at: <https://physionet.org/physiotools/wag/signal-5.htm#sect9>

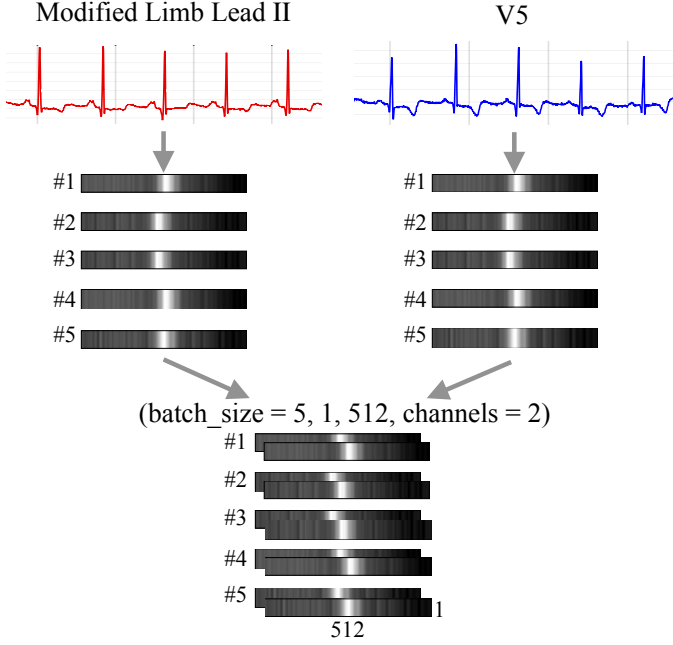


Fig. 2. Reconstruction of two-lead ECG data using MIT-BIH Record 100 as a case. The output data is organized in the form of ($batch_size = 5, height = 1, width = 512, channel = 2$).

two sub-datasets²: DS1 and DS2. According to the evaluation scheme recommended by AAMI, the VEB and SVEB can be evaluated separately using the two subsets: DS2-v and DS2-s³. The first 5 minutes of the ECG records (DS1 and DS2) are used as the training set, which builds up the common part and the patient-specific part, and the remaining 25 minutes of each segment are used as test set. The numbers of samples in AAMI classes for the training set are 13480 (N), 258 (S), 1083 (V), 175 (F), 0 (Q). The numbers are 65524 (N), 2668 (S), 5828 (V), 618 (F), 13 (Q) for the test set.

5) *Data Equilibrium*: To prevent unbalanced samples from causing an incorrect propensity when training the model, we applied the method of label shuffling method [35] to augment the data for each training set. Simply applying the duplication to upsample the lack-of-sample classes will not increase the amount of substantial information, so we use the SMOTE method [36] to apply data augmentation to the lack-of-sample classes (SVEB) and edit the Tomek links [37] for all the training set, mainly to reduce unnecessary N -class samples, enhancing the generalization ability of the trained network model to find a balanced performance for the easy-to-confuse N and S classes. In addition, adopting both duplication and downsampling can lighten the gravity of the overfitting problem. After the augmentation, the final number of samples used for training after balance is as follows: 10000 (N), 8000 (S), 8000 (V), 4000 (F), 0 (Q). The class Q , excluded in

²DS1 contains data from ECG recordings: 101, 105, 106, 108, 109, 111, 112, 113, 115, 116, 118, 119, 121 and 122; DS2 contains data from ECG recordings: 200, 201, 202, 203, 205, 207, 208, 209, 210, 212, 213, 214, 215, 219, 220, 221, 222, 223, 228, 230, 231, 232, 233 and 234.

³DS2-v contains data from: 200, 202, 210, 213, 214, 219, 221, 228, 231, 233 and 234; DS2-s contains data from: 200, 202, 210, 212, 213, 214, 219, 221, 222, 228, 231, 232, 233 and 234.

augmentation procedures due to its extremely small number of samples, is not consider as main index of the evaluation.

III. MODELS

1) *Resnet for a single channel — model A*: This model is built with a single channel of ECG input. We performed experiments on each lead of the signal. We adopt the residual-v2 blocks [38] structure to build the ECG signal classification network model. The residual learning framework structure is a network with a shortcut, which solves the issue of training a deeper neural network model being difficult. We build a series of deep neural networks with residual blocks. See Table I for details of the models.

2) *Resnet for both channels — model B*: We build a two-channel ECG inputs model, which takes the advantage of the information gain by increasing the feature dimensions of the input that is organized in the form shown in Fig. 2. In addition, we attempt to establish relationships between different channels (integrating information from different channels) through the architecture of the plain residual CNN. The backbone structure of this model is the same as that of model A shown in Table I.

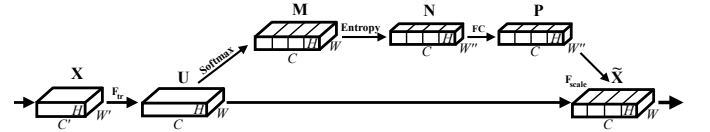


Fig. 3. Information-based squeeze and excitation block. H stands for the height of the feature map. W is the width of the feature map. W' and W'' indicates a different numerical value from W . And C is the number of channels of the feature map. Bold characters $XUMNP$ are names of the matrices. F_{tr} is the residual block in the proposed model and F_{scale} is the element-wise multiply with the broadcast nature in Python between the P and U matrices.

3) *Attention model for both channels — model C*: Compared with model B, the major improvement of this model is that a channel-attention network structure named as ISE-block, is embedded to realize channel-wise feature maps recalibration. The backbone structure of this model is the same as those of model A and model B shown in Table I. An ISE-block is established on the output feature maps of different channels, and it attempts to describe the difference in the importance and richness of valid information in different feature maps of the same hidden layer and attempts to weight the features accordingly. For the task of multi-channel ECG

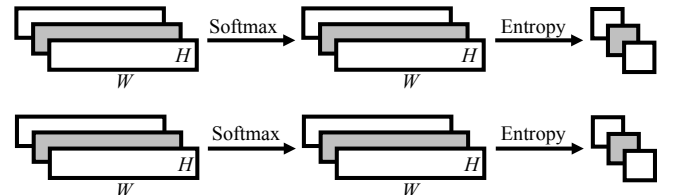


Fig. 4. Softmax and Entropy block. A brief schematic of the softmax and entropy implementation of the data batch in form of ($batch_size = 2, height = H, width = W, channel = 3$).

TABLE I
BACKBONE NETWORK STRUCTURES WITH VARIOUS DEPTH FOR MODEL COMPLEXITY MINING TOWARDS ECG CLASSIFICATION TASK

Layer	output	11-layer	14-layer	17-layer	20-layer	23-layer	26-layer
conv1	1×256	1x4, 8, stride 2					
		1x3 max pool, stride 2					
block1	1×64	$\begin{bmatrix} 1 \times 1, & 8 \\ 1 \times 3, & 8 \\ 1 \times 1, & 16 \end{bmatrix} \times 1$	$\begin{bmatrix} 1 \times 1, & 8 \\ 1 \times 3, & 8 \\ 1 \times 1, & 16 \end{bmatrix} \times 1$	$\begin{bmatrix} 1 \times 1, & 8 \\ 1 \times 3, & 8 \\ 1 \times 1, & 16 \end{bmatrix} \times 1$	$\begin{bmatrix} 1 \times 1, & 8 \\ 1 \times 3, & 8 \\ 1 \times 1, & 16 \end{bmatrix} \times 1$	$\begin{bmatrix} 1 \times 1, & 8 \\ 1 \times 3, & 8 \\ 1 \times 1, & 16 \end{bmatrix} \times 1$	$\begin{bmatrix} 1 \times 1, & 8 \\ 1 \times 3, & 8 \\ 1 \times 1, & 16 \end{bmatrix} \times 1$
block2	1×32	$\begin{bmatrix} 1 \times 1, & 16 \\ 1 \times 3, & 16 \\ 1 \times 1, & 32 \end{bmatrix} \times 1$	$\begin{bmatrix} 1 \times 1, & 16 \\ 1 \times 3, & 16 \\ 1 \times 1, & 32 \end{bmatrix} \times 1$	$\begin{bmatrix} 1 \times 1, & 16 \\ 1 \times 3, & 16 \\ 1 \times 1, & 32 \end{bmatrix} \times 1$	$\begin{bmatrix} 1 \times 1, & 16 \\ 1 \times 3, & 16 \\ 1 \times 1, & 32 \end{bmatrix} \times 2$	$\begin{bmatrix} 1 \times 1, & 16 \\ 1 \times 3, & 16 \\ 1 \times 1, & 32 \end{bmatrix} \times 2$	$\begin{bmatrix} 1 \times 1, & 16 \\ 1 \times 3, & 16 \\ 1 \times 1, & 32 \end{bmatrix} \times 2$
block3	1×16	$\begin{bmatrix} 1 \times 1, & 32 \\ 1 \times 3, & 32 \\ 1 \times 1, & 64 \end{bmatrix} \times 1$	$\begin{bmatrix} 1 \times 1, & 32 \\ 1 \times 3, & 32 \\ 1 \times 1, & 64 \end{bmatrix} \times 1$	$\begin{bmatrix} 1 \times 1, & 32 \\ 1 \times 3, & 32 \\ 1 \times 1, & 64 \end{bmatrix} \times 2$	$\begin{bmatrix} 1 \times 1, & 32 \\ 1 \times 3, & 32 \\ 1 \times 1, & 64 \end{bmatrix} \times 2$	$\begin{bmatrix} 1 \times 1, & 32 \\ 1 \times 3, & 32 \\ 1 \times 1, & 64 \end{bmatrix} \times 2$	$\begin{bmatrix} 1 \times 1, & 32 \\ 1 \times 3, & 32 \\ 1 \times 1, & 64 \end{bmatrix} \times 3$
block4	1×8		$\begin{bmatrix} 1 \times 1, & 64 \\ 1 \times 3, & 64 \\ 1 \times 1, & 128 \end{bmatrix} \times 1$	$\begin{bmatrix} 1 \times 1, & 64 \\ 1 \times 3, & 64 \\ 1 \times 1, & 128 \end{bmatrix} \times 1$	$\begin{bmatrix} 1 \times 1, & 64 \\ 1 \times 3, & 64 \\ 1 \times 1, & 128 \end{bmatrix} \times 1$	$\begin{bmatrix} 1 \times 1, & 64 \\ 1 \times 3, & 64 \\ 1 \times 1, & 128 \end{bmatrix} \times 2$	$\begin{bmatrix} 1 \times 1, & 64 \\ 1 \times 3, & 64 \\ 1 \times 1, & 128 \end{bmatrix} \times 2$
	1×1	global average pooling					

classification, we argue that channel-wise learning can be used to improve the model’s ability to express the multi-lead ECG data. Compared with Hu’s work [39], we build a more complex channel-attention structure, through which the information-based feature calibration is realized. The following describes the details of this channel-wise structure.

According to our network definition, the data format of the feature maps can be expressed in the matrix form of $(batch_size, height, width, channel)$. For a clear display of the ISE-block, let $batch_size = 1$, and then the ISE-block is as shown in Fig. 3. It is possible to refer to the feature maps obtained by the forward propagation of all the ECG samples in the input batch corresponding to the layer l of the convolutional neural network model as F_l . Therefore, $F_l[i], i = 0 \dots (batch_size - 1)$ represents a set of feature maps which are obtained by the forward propagation of the i -th ECG sample in an input batch to the l -th layer in the neural network model, which has a format of $(height, width, channel)$. As shown in Fig. 4, we implement the softmax function to transform the feature map U to feature map M in Fig. 3. Given the general implementation of softmax formula as follows:

$$\sigma(z_j) = \frac{e^{z_j}}{\sum_{k=1}^K e^{z_k}} \quad (2)$$

We build the softmax structures for the feature map derived by the forward propagation of the input batch. The feature maps taken into consideration for the softmax computation can be defined as follows: Using the $F_l[i]$ defined above as the base, the c -th channel of the set of feature maps is defined as $F_l[i][c]$, and the value of the j -th node in $F_l[i][c]$ is set as $F_l[i][c][j]$. Thus, the softmax computation can be presented by the following equation:

$$\sigma(F_l[i][c][j]) = \frac{e^{F_l[i][c][j]}}{\sum_{j=0}^{W \times H - 1} e^{F_l[i][c][j]}} \quad (3)$$

where the σ is the symbolic representation of the softmax function. The entropy structure is shown in the M to N section of Fig. 3, which is named as ‘‘Extraction’’. As shown in the Fig. 4, the softmax layers proposed above do not change the data format of the feature map in the convolutional neural

network. Given the symbol $F_l[i][c][j]$ as above, the entropy is computed as:

$$H(z) = - \sum_{j=0}^{W \times H - 1} p(F_l[i][c][j]) \log p(F_l[i][c][j]) \quad (4)$$

where z stands for the random variable of the c -th channel of the l -th hidden layer. It should be noted that the above formula is obtained on the premise that several approximations are applied and will be discussed in detail in the appendixes. The fully-connected layers (FC layers) work as a ‘‘weight

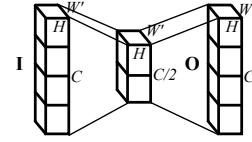


Fig. 5. Full-connected layers with decay ratio=2.

calibrator’’ for the information embedded vector shown in Fig. 5. In the design of this structure, the initial motivation is that the training of two FC layers can compensate for the inherent shortcomings of the structure N’s deficiency in mapping its values to the relative valid information quantity of $F_l[i][c]$. We also refer to the two standards proposed in the SE-net [39]: First, the structure should be capable of learning a nonlinear interaction between channels and second, it must learn a non-mutually-exclusive relationship. The number of input nodes in the FC layers is equal to the number of its output nodes, which is equal to the number of channels in the ISE-block input feature map. Assuming that the number of channels in the ISE-block’s input feature map is c , the ratio (r) represents the decay rate of the channels input, then the number of hidden nodes (n) is determined by the following formula:

$$n = \lfloor c/r \rfloor \quad (5)$$

$$r = 2, c \leq 8 \quad \text{or} \quad r = 8, c > 8.$$

where $\lfloor a \rfloor$ stands for the integer (*floor*) of a . Finally, we use the structure named P in Fig. 3 as a fuzzy measure of the relative validity of the information extracted from each feature map in a certain layer.

IV. TRAINING

1) *Training objective*: The open source framework TensorFlow is adopted for all the experiments conducted, and the *softmax_cross_entropy_with_logits_v2* function in TensorFlow is utilized to calculate the cross entropy. The l2-loss for the weights in the network is added to the total loss to resist the overfitting problem.

2) *Optimizer selection*: The adam optimizer and the momentum optimizer are considered in our experiments. The adam optimizer always performs better than the momentum optimizer in the training process, and it produces good test results in most cases. In general, models optimized with momentum have stronger generalization capabilities in ECG classification issues in testing procedures. The optimizer related parameters are set as follows. For the adam optimizer: beta1: 0.9, beta2: 0.999, and epsilon: $1 \times e^{-8}$. For the momentum optimizer: momentum: 0.9, and use_nesterov=False.

3) *Learning rate scheme*: We tested two methods for decreasing the learning rate—the piecewise constant learning rate and exponential decay learning rate, and found that the exponential decay learning rate can achieve better results in the training set, yet the piecewise-constant learning always yields better results with carefully designed learning rates and learning rate boundaries in testing procedures. The relevant parameters are set as follows: For exponential-decay, decay steps: 1 epoch, and decay rate: 0.97; For the piecewise constant, learning rate list: 1×10^{-3} , 5×10^{-4} , 1×10^{-4} , 5×10^{-5} , 1×10^{-5} , 5×10^{-6} , and 1×10^{-6} and the learning rate boundaries: 3-epochs, 10-epochs, 20-epochs, 40-epochs, 80-epochs, and 160-epochs. The hyper-parameters listed above are set as a base for most of the ablation experiments. Fine-tuning is necessary for different backbone selections.

4) *Training strategy*: All the models in this article are trained with Nvidia Tesla P100 GPU, and the code is written in Python 3.6.5. In the subject-oriented experiments, the method of cross-validation on the training and validation sets is used to obtain relatively reliable hyper-parameters and to obtain a more generalized model that does not depend on the quality of data partitioning. In addition to the above strategies, we introduce the “early stop” method to explore the best performance to the intractable problem of misclassifying S into N and finally reach a balance between the chosen indicators: sensitivity and precision. Specifically, we perform model evaluation on the validation set per epoch training steps. The performance of each model on the dataset per epoch is recorded by our program, and the checkpoints with better performances are saved automatically.

5) *Assessment indicators*: We evaluated the results obtained from the experiments according to the evaluation indicators recommended in [40] and with reference to the evaluation methods in other papers for ECG classification in the mitdb. The final evaluation indicators are as follows:

$$Acc = \frac{TP + TN}{TP + TN + FP + FN} \quad (6)$$

$$Sen = \frac{TP}{TP + FN} \quad (7)$$

$$Spe = \frac{TN}{TN + FP} \quad (8)$$

$$Ppr = \frac{TP}{TP + FP} \quad (9)$$

$$MCC = \frac{TP/N - S \times P}{\sqrt{PS(1-S)(1-P)}} \quad (10)$$

where TP is true positive, TN is true negative, FP is false positive and FN is false negative, MCC is the Matthews correlation coefficient, $N = TN + TP + FN + FP$, $S = (TP + FN)/N$, and $P = (TP + FP)/N$.

TABLE II
PATIENT-SPECIFIC CLASSIFICATION PERFORMANCE OF BACKBONE NETWORKS ON DIFFERENT LEAD CONFIGURATIONS¹

Models	VEB				SVEB			
	Acc	Sen	Spe	Ppr	Acc	Sen	Spe	Ppr
Resnet-11 ²	98.3	96.1	98.6	90.1	97.1	68.0	98.9	79.2
Resnet-11 ³	94.0	91.8	94.3	68.3	96.5	65.8	98.4	72.0
Resnet-11 ⁴	98.6	94.2	99.2	93.7	97.2	69.5	98.9	79.8
Resnet-14 ²	98.6	93.5	99.3	94.4	97.1	69.0	98.9	79.1
Resnet-14 ³	97.3	91.5	98.1	86.6	97.0	66.3	98.9	79.7
Resnet-14 ⁴	98.7	95.4	99.1	93.5	97.4	69.2	99.2	84.0
Resnet-17 ²	98.6	93.9	99.2	93.8	97.1	69.0	98.9	79.3
Resnet-17 ³	98.0	92.7	98.7	90.2	97.1	66.0	99.0	80.8
Resnet-17 ⁴	98.9	95.8	99.3	94.8	97.3	68.4	99.1	83.3
Resnet-20 ²	98.6	94.9	99.1	93.2	97.1	70.4	98.8	78.2
Resnet-20 ³	98.0	91.8	98.8	91.3	97.1	66.6	99.0	80.6
Resnet-20 ⁴	99.0	95.4	99.5	96.4	97.3	67.8	99.2	83.8
Resnet-23 ²	98.8	96.5	99.1	93.3	97.1	69.0	98.8	78.5
Resnet-23 ³	98.4	92.3	99.2	93.9	97.2	67.5	99.1	82.4
Resnet-23 ⁴	99.2	96.6	99.6	96.9	97.2	69.8	98.9	80.6
Resnet-26 ²	98.9	95.8	99.3	95.0	97.2	68.3	99.0	80.5
Resnet-26 ³	98.5	93.2	99.3	94.4	97.2	65.9	99.1	82.8
Resnet-26 ⁴	99.1	95.7	99.6	96.8	97.3	69.3	99.0	81.8

¹ The comparison results are all based on DS2-v for VEB detection and DS2-s for SVEB detection.

² The VEB and SVEB detection results are based on the lead MLII.

³ The VEB and SVEB detection results are based on the lead V1.

⁴ The VEB and SVEB detection results are based on both leads.

V. RESULTS

According to the AAMI recommendations, the issues of VEB and SVEB detection are considered individually. The results for a set of control experiments are shown in Table II above, which relates to different ECG lead configurations and various depths of the backbone 1D Resnet. The experimental results from the models that accept both ECG leads always perform better in overall performance of VEB and SVEB detection. Most results from models using lead MLII surpass those from the models using lead V1 signal as input. Shallower models such as Resnet-11 and Resnet-14 generally have comparable results with those of deeper models in SVEB classification, while they perform poorly in VEB classification. Although data augmentation is implemented mainly for SVEB, VEB still has a greater information abundance than that of SVEB. The shallower models’ complexity is not sufficient to converge to VEB’s real distribution. Furthermore, shallower models are more likely to achieve similar results to those of deeper models in sensitivity, but do not perform equally well in precision (N is misclassified as S), indicating that the class N, with greater information richness, requires deeper networks for full encoding and decoding. Table III reveals the results

from the models embedded with the proposed information-based channel-wise structure. The test performance indicators Sen and Ppr of SVEB are taken into consideration for model selection. The results in Table III are derived by the following criterion: Set the model performance index as: $index = Sen + Ppr$, in which the sensitivity and precision are computed from the SVEB test performance. Candidate models with top ten index values are selected from the checkpoints. The model checkpoint that provides the best MCC on SVEB is chosen for display. The deeper ISEnet tends to achieve better Ppr values of SVEB and VEB during the training process with the decrease of Sen as a sacrifice, which can be explained by the great disparity in terms of information quantity between the N class and S class.

TABLE III
PATIENT-SPECIFIC CLASSIFICATION PERFORMANCE OF PROPOSED NETWORKS ON DIFFERENT BACKBONE CONFIGURATIONS¹

Models	VEB				SVEB			
	Acc	Sen	Spe	Ppr	Acc	Sen	Spe	Ppr
ISEnet-11	99.0	96.2	99.3	95.1	97.1	70.2	98.8	78.9
ISEnet-14	99.4	97.1	99.7	97.6	97.7	70.9	99.4	87.6
ISEnet-17	99.0	97.0	99.3	94.9	97.5	71.9	99.1	83.0
ISEnet-20	99.1	96.1	99.5	96.5	97.4	69.4	99.2	84.1
ISEnet-23	99.3	94.8	99.8	98.8	97.4	70.2	99.1	82.6
ISEnet-26	99.2	95.6	99.7	97.6	97.5	70.7	99.1	83.7

¹ The comparison results are all based on DS2-v for VEB detection and DS2-s for SVEB detection.

For the proposed attention model, Table IV presents the confusion matrix of ECG beat classification test results for all the 38 records of train and test sets. The test result for 24 test records (DS2) is shown in parentheses. The comparison between the chosen proposed model and the results in other works is shown in Table V. Our partitioning method of the benchmark training set that consists of common part and patient-specific part and test set are in consistent with the compared algorithms during the comparison implementation. Under the selected data division scheme, the base performance of the ISEnet-14, which is the best performing model in our trials, is compared with four state-of-the-art algorithms [10], [24], [25], and [26] which conform to the AAMI standard. Compared with these works, the proposed model achieves higher Acc and comparable Sen in SVEB classification, and in the VEB classification issue, our model presents better results in the Sen index.

TABLE IV
CONFUSION MATRIX OF ISENET-14 TESTING ON MIT-BIH RECORDS

Label	Prediction					Σ
	N	S	V	F	Q	
N	77950 (49526)	507 (306)	377 (174)	170 (162)	0 (0)	79004 (50168)
S	934 (885)	1904 (1840)	77 (76)	11 (11)	0 (0)	2926 (2812)
V	284 (193)	32 (19)	6543 (5463) [6572]	52 (49) [23]	0 (0)	6911 (5724)
F	46 (44)	1 (1)	48 (48) [19]	698 (696) [727]	0 (0)	793 (789)
Q	4 (4)	0 (0)	9 (3)	0 (0)	0 (0)	13 (7)
Σ	79218 (50652)	2444 (2166)	7054 (5764)	931 (918)	0 (0)	89647 (59500)

VI. DISCUSSION

1) *More channels can be better*: The results listed above show that utilizing dual-lead ECG as the input benefits the ECG classification tasks. This is also confirmed in literature [18] and [19]. Fig. 7 is used to characterize the model

complexity and the overall model performance in MCC index on the ECG classification task in the ablation study. Models that accept dual leads as input surpass the performance of those accept single lead in ECG classification tasks with only a small increase in model complexity. Reasonably increasing the dimension of the input features on the premise of intensively debugging the hyper-parameters and appropriately applying training techniques will greatly improve the performance of the model and resist the tendency of over-fitting.

TABLE V
VEB AND SVEB CLASSIFICATION PERFORMANCE AND COMPARISON WITH FOUR STATE-OF-THE-ART LITERATURES

Models	VEB				SVEB			
	Acc	Sen	Spe	Ppr	Acc	Sen	Spe	Ppr
Hu et al.	94.8	78.9	96.8	75.8	N/A	N/A	N/A	N/A
Jiang and Kong ²	98.8	94.3	99.4	95.8	97.5	74.9	98.8	78.8
Jiang and Kong ³	98.1	86.6	99.3	93.3	96.6	50.6	98.8	67.9
Ince et al. ²	97.9	90.3	98.8	99.2	96.1	81.8	98.5	63.4
Ince et al. ³	97.6	83.4	98.1	87.4	96.1	62.1	98.5	56.7
Ince et al. ⁴	98.3	84.6	98.7	87.4	97.4	63.5	99.0	53.7
Kiranyaz et al. ²	98.9	95.9	99.4	96.2	96.4	68.8	99.5	79.2
Kiranyaz et al. ³	98.6	95	98.1	89.5	96.4	64.6	98.6	62.1
Kiranyaz et al. ⁴	99.0	93.9	98.9	90.6	97.6	60.3	99.2	63.5
ISEnet-14 ²	98.9	96.7	99.2	94.5	97.1	68.0	98.9	79.1
ISEnet-14 ³	98.4	95.2	98.7	89.1	96.8	63.3	98.4	66.9
ISEnet-14 ⁴	98.6	94.5	98.9	88.2	97.6	63.1	98.7	62.8

² The comparison results are based on DS2-v for VEB detection and DS2-s for SVEB detection.

³ The VEB and SVEB detection results are compared for DS2 only.

⁴ The VEB and SVEB detection results of the proposed models for testing part of DS1 and DS2.

2) *Comprehension of the layers' function through excitation values*: To study the functions of different ISE-blocks embedded in the middle of the backbone networks, the ISEnet-14 is selected as a base and tested using randomly selected 500 samples from each class except Q in the test datasets. Then, we plot the average excitation values characterized by matrix P in the Fig. 3 of all the samples, as shown in Fig.6. The above sample selection process is repeated multiple times to ensure that the pattern of the excitation values we obtain do not depend on the contingency of selecting the test data. Two observations are made from the visualization of the proposed structures. As shown in subfigure a in Fig.6, the excitation values of Block1 Unit1 distributes between 0.313 and 0.834, with merely six of the sixteen channels lying under 0.5, revealing that most channels values characterizing the general features are preserved in shallower layers of the network. In the deeper depths of the model, the range of the excitation values stretches to 0.0171 – 0.979, which indicates significant suppression and excitation of different channels on the feature map. That is, the main function of the shallow layers is to extract general information with few differences among categories, and the deeper layers are majorly responsible for the compression and integration of the relevant information towards the sample types. Furthermore, for each embedded ISE-block (a – b) in Fig.6, channel-wise activation values are adopted to calculate the mean square deviation defined below for any two classes:

$$MSD_{m,n} = \frac{M}{C} \sum_{i=0}^{C-1} (m_i - n_i)^2 \quad (11)$$

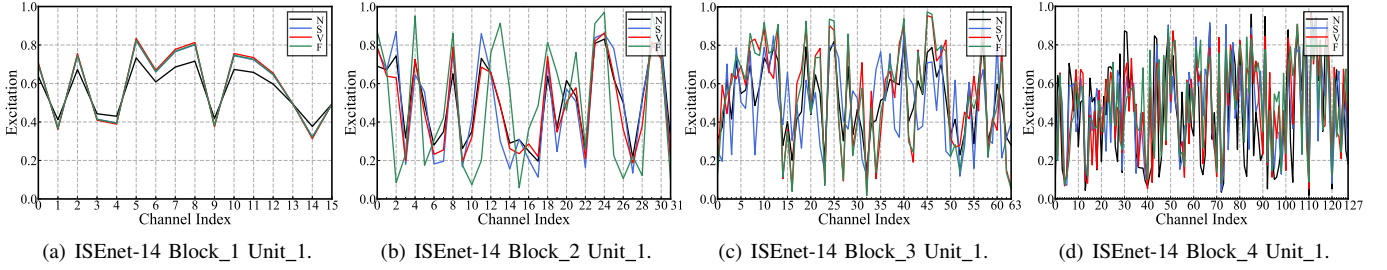


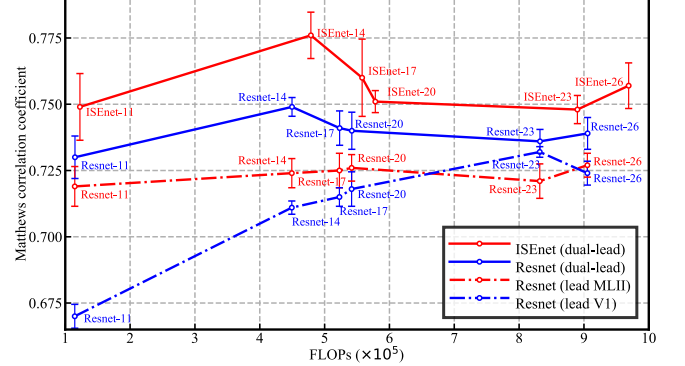
Fig. 6. Excitation value induced by structure P in Figure 3 of the various blocks of ISEnet-14 on N, S, V, F samples from the test set of mitdb. See Table I for details of ISEnet-14 block and unit configurations.

where C denotes the number of channels depicted in Fig.6, M denotes the multiplier factor and is set to 100, and m and n stands for the two classes involved in the computation. For N-S, the MSD values from subfigure a to subfigure d are 0.329, 0.821, 2.425, and 3.764. For N-V: they are 0.442, 0.545, 2.909, and 4.052. For N-F, S-F and V-F, the MSD values computed from the block2 are the highest. For S-V, the MSD values from the block3 are the highest. Ignoring the effect of the back-propagation algorithm on model convergence, we argue that the MSD values derived above partly characterize the relationship between the information flow on the selected two classes and the ability for model segments to encode and decode, which sliced from the input layer to the layer that used to calculated MSD values. Taking $MSD_{v,f}$ as an case, we truncate the trained ISEnet-14 model at the end of block2 and append it with a convolutional layer and a global average pooling layer to form a model towards V and F classification. The parameters in the segmented part are finetuned with a smaller learning rate, and the appended layers are trained with the selected two classes. The refined results derived from the two combined models are shown in Table IV enclosed in square brackets. The above phenomenon and its analysis results reveal that for the ECG classification task, the smallest network segment that is advantageous for the distinction between the two types of ECG classes can be obtained by calculating the MSD values. The reasonable use of the network segment selected according to the MSD index can improve the accuracy of the ECG classification issue and the generalization ability of the corresponding model.

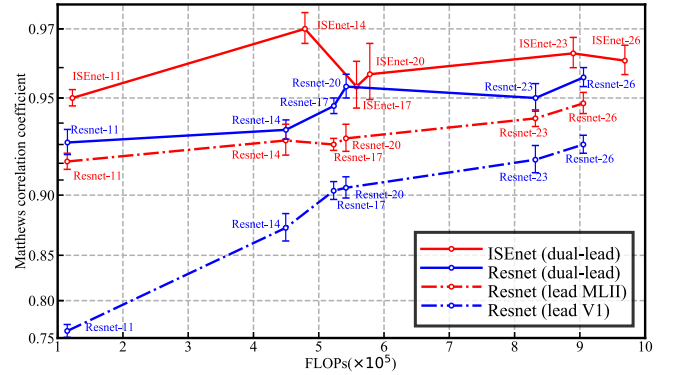
3) *Backbone structures mining*: The classic resnet-v2 structure and three variants of the ISE-block are shown in Fig. 8. In this study, the standard structure of the ISE-block is chosen. We made preliminary attempts on the other two variants, and they could also perform well in the ECG classification task. This reveals that the ISE-block can be embedded as a general unit in the network. Other network backbones and ISE-variants may be able to achieve similar results in solving the classification task, which is beyond the scope of this study.

VII. CONCLUSION

The backbone network structures adopted are a “one-stage” training strategy, which can realize automatic feature extraction to achieve better robustness and higher adaptability in ECG classification issues compared with methods involving manually extracting features. A set of data partitioning and reconstruction schemes is proposed for applying dual-lead



(a) SVEB detection results in Matthews correlation coefficient of different models with related FLOPs.



(b) VEB detection results in Matthews correlation coefficient of different models with related FLOPs. The y scale is processed using the logit function for better display of the contrast of different models’ performances.

Fig. 7. The relationship between model complexity and model performance using Matthews correlation coefficient as an index in our ablation study. The ranges of the error bars are calculated by $M \pm std$, where M and std are mean value and standard deviation from the results of 6 repetitive experiments of the same model.

signals in the mitdb for the neural networks. The proposed scheme conforms to the AAMI standard and fully satisfies the requirements of deep neural network algorithms. With reference to the information bottleneck theory, we derive the possibility that applying statistics in the feature maps of the backbone model helps quantify the “valid information quantity”, which is used as an index to monitor the neural network training quality and to help comprehend the relationship between the model structures and its functionalities. The perspective that utilizing multi-channel signals can help train better generalized deep networks with superior performance in

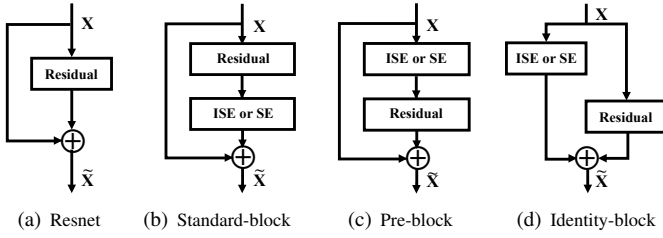


Fig. 8. Resnet block together with standard ISE block and its variants.

ECG classification tasks is proven through a series of control experiments. We design a structure based on a channel attention mechanism, which can effectively realize the channel-wise weights recalibration (excitation and suppression). The proposed model has the potential to use more leads for the analytical diagnosis of more complex heart diseases.

However, it should be noted that the ECG signal is a time sequence, while the proposed network structure fails to utilize the characteristics of long-term time series of the signal, which may lead to the failure of the analysis of heart diseases characterized by episode-level features. In addition, the performance of our model is limited by the quality of the beat-by-beat segmentation algorithm and the signal preprocessing schema. Due to the neural network’s black-box nature and the simplifications made in the design of the ISE structures, it is not yet possible to strictly prove the validity of the designed structures in theory.

In the future, we will use RNN and its variants as the backbone to model the long-term ECG signals, and to figure out the dependency between the more complicated heart diseases with its lead configurations. We will go further to prove the argument that integrating the MSD index with the network model design will benefit the performance of the classification model.

APPENDICES

1) *Go deeper in the ISE-block*: The idea behind the proposed ISE-block comes from the expression of the hidden layers in neural networks based on the information bottleneck theory in [41] and [42]. We argue that neural networks can be interpreted as information encoding and decoding, which are structures that integrate and process information. These two functions are implemented simultaneously in any hidden layer during the training of the neural network. Schwartz-Ziv and Zaslavsky provides a good mathematical explanation of the above viewpoint [41]: Let T_i represents the i -th hidden layer, and the T_i is uniquely mapped to a point in the information-plane with coordinates $(I(X; T_i), I(T_i; Y))$. In [42], Tishby et al. argue that the efficiency of the network’s hidden layers can be quantified by the amount of information it retains on the input variable. Thus, we consider trying to quantify the flow of information in a neural network by grafting a structure in a neural network. The quantified results are applied to different channels of the original feature maps to enhance the fusion of neural network channel features, to achieve better results in multi-channel ECG classification modeling tasks.

We use the mutual information to quantify the valid information of T_i , which can be thought of as the amount of information about another random variable contained in a

random variable. The mutual information of any two random variables X and Y can be defined as:

$$I(X; Y) = D_{KL}[p(x, y) \| p(x)p(y)] = H(X) - H(X|Y) \quad (12)$$

where $p(x, y)$ is the joint distribution of x and y , $D_{KL}(p \| q)$ is the KL divergence, and $H(X)$ and $H(X|Y)$ are the entropy and conditional entropy. First, we derive the expression of the “valid information expression” based on the structure of deep neural network (DNN). Let X be the input of the DNN, and let Y be the random variable identified by the label distribution, and T_i represents the whole i -th hidden layer, which can be treated as a single random variable and represented by $P(T_i|X)$ and $P(Y|T_i)$ distributions [41]. Thus, $I(T_i; Y)$ is the quantity of information about the random variable Y contained in T_i .

The “valid information expression” of a CNN is derived in the following part. The convolution operation is a reconstructed sparse form of the fully-connected structure in a DNN. For a given feature map T_i with 3×3 nodes named $t_{i0}, t_{i1} \dots t_{i8}$, a kernel K_i with 2×2 nodes named k_{i0}, k_{i1}, k_{i2} and k_{i3} , and the resulting output with 4 nodes named o_{i0}, o_{i1}, o_{i2} and o_{i3} , taking the output node o_{i0} as an instance, the convolution ($stride = 1$) on the input T_i can be transformed into the following equation:

$$o_{i0} = t_{i0} \times k_{i0} + t_{i1} \times k_{i1} + t_{i2} \times 0 + t_{i3} \times 0 + t_{i4} \times k_{i2} + t_{i5} \times k_{i3} + t_{i6} \times 0 + t_{i7} \times 0 + t_{i8} \times 0 \quad (13)$$

For the i -th hidden layer in a CNN model expressed as T_i , let j denote one of its total c channels; thus, $T_i[j]$ is the j -th feature map in T_i , and it is derived by the convolution of the j -th kernel and the $T_{i-1}[j]$. The output feature map of a certain kernel is combined by weight sharing and sparse connection, and is directly computed through element-wise addition. Given the relationship between CNN and DNN derived above, we argue that each $T_i[j]$ is a single random variable, and the “valid information expression” can be derived as $I(T_i[j]; Y)$. Thus, we can use the expression to get the relative “importance score” between different channels of the same layer of the convolutional neural network. However, in the training process of CNN models, the distribution of a hidden layer $P(T_i[j])$ is hard to calculate, and it is not possible to flush all the training data into the model to approach the true distribution, which motivates us to seek an alternative that is both computationally friendly and close to the original mathematical principle. We made several simplifications for the expression: $I(T_i[j]; Y) = H(T_i[j]) - H(T_i[j]|Y)$, in which $H(T_i[j])$ and $H(T_i[j]|Y)$ are both hard to estimate, we adopt its symmetrical form: $I(Y; T_i[j]) = H(Y) - H(Y|T_i[j])$, in which the $H(Y)$ is a constant and is fully determined by the label distribution. Thus the expression can be simplified by cutting off its constant part. Given $H(H|X) = \sum_x p(x)H(Y|X = x)$, the information expression can be computed as:

$$H(Y|T_i[j]) = - \sum_{t_i[j], y} p(t_i[j], y) \log p(y|t_i[j]) \quad (14)$$

where $t_i[j]$ denotes the observation value of the random variable $T_i[j]$. A single forward propagation of a neural network

can only yield one observation $t_i[\hat{j}]$ in the $T_i[j]$ distribution. The distribution of Y can be approximated by observing the label distribution. However, we still cannot directly solve the two probability values in (14). Through the back propagation in training each neural network, the distribution of a certain hidden layer converges to its true distribution, upon which we can implement quantification and optimization operations on. Moreover, the expression of (14) provides us an approximate way of measuring the quantity of the information flow. That is, we can provide channel recalibration information for the training process by observing the internal numerical statistics of $t_i[\hat{j}]$ within each inference. Finally, we use two FC layers as calibration structures for channel-wise learning to compensate for the simplifications above.

REFERENCES

- [1] S. Jayaraman, V. Sangareddi, R. Periyasamy, and J. Joseph, "Modified limb lead ecg system effects on electrocardiographic wave amplitudes and frontal plane axis in sinus rhythm subjects," *The Anatolian Journal of Cardiology*, vol. 17, pp. 46–54, 01 2017.
- [2] R. Mark and G. Moody, "Mit-bih arrhythmia database directory," Cambridge, MA, USA: MIT, 1988.
- [3] S. Osowski, L. T. Hoai, and T. Markiewicz, "Support vector machine-based expert system for reliable heartbeat recognition," *IEEE Transactions on Biomedical Engineering*, vol. 51, no. 4, pp. 582–589, April 2004.
- [4] D. A. Coast, R. M. Stern, G. G. Cano, and S. A. Briller, "An approach to cardiac arrhythmia analysis using hidden markov models," *IEEE Transactions on Biomedical Engineering*, vol. 37, no. 9, pp. 826–836, Sep. 1990.
- [5] V. X. Afonso, W. J. Tompkins, T. Q. Nguyen, and S. Luo, "Ecg beat detection using filter banks," *IEEE Transactions on Biomedical Engineering*, vol. 46, no. 2, pp. 192–202, Feb 1999.
- [6] O. T. Inan, L. Giovangrandi, and G. T. A. Kovacs, "Robust neural-network-based classification of premature ventricular contractions using wavelet transform and timing interval features," *IEEE Transactions on Biomedical Engineering*, vol. 53, no. 12, pp. 2507–2515, Dec 2006.
- [7] P. de Chazal, M. O'Dwyer, and R. B. Reilly, "Automatic classification of heartbeats using ecg morphology and heartbeat interval features," *IEEE Transactions on Biomedical Engineering*, vol. 51, no. 7, pp. 1196–1206, July 2004.
- [8] M. Kumar Das and S. Ari, "Ecg beats classification using mixture of features," *International Scholarly Research Notices*, vol. 2014, 09 2014.
- [9] S. Sabut, S. Sahoo, B. Kanungo, and S. Behera, "Multiresolution wavelet transform based feature extraction and ecg classification to detect cardiac abnormalities," *Measurement*, vol. accepted, pp. 55–66, 05 2017.
- [10] S. Kiranyaz, T. Ince, and M. Gabbouj, "Real-time patient-specific ecg classification by 1-d convolutional neural networks," *IEEE Transactions on Biomedical Engineering*, vol. 63, no. 3, pp. 664–675, March 2016.
- [11] S. S. Xu, M. Mak, and C. Cheung, "Towards end-to-end ecg classification with raw signal extraction and deep neural networks," *IEEE Journal of Biomedical and Health Informatics*, pp. 1–1, 2018.
- [12] "Automated detection of arrhythmias using different intervals of tachycardia ecg segments with convolutional neural network," *Information Sciences*, vol. 405, pp. 81 – 90, 2017.
- [13] "Application of stacked convolutional and long short-term memory network for accurate identification of cad ecg signals," *Computers in Biology and Medicine*, vol. 94, pp. 19 – 26, 2018.
- [14] "Characterization of coronary artery disease using flexible analytic wavelet transform applied on ecg signals," *Biomedical Signal Processing and Control*, vol. 31, pp. 301 – 308, 2017.
- [15] "Application of higher-order spectra for the characterization of coronary artery disease using electrocardiogram signals," *Biomedical Signal Processing and Control*, vol. 31, pp. 31 – 43, 2017.
- [16] "Automated detection of coronary artery disease using different durations of ecg segments with convolutional neural network," *Knowledge-Based Systems*, vol. 132, pp. 62 – 71, 2017.
- [17] D. Mirvis, S. Berson *et al.*, "Instrumentation and practice standards for electrocardiographic monitoring in special care units. a report for health professionals by a task force of the council on clinical cardiology, american heart association [published erratum appears in *circulation* 1989 aug; 80(2):a85]," *Circulation*, vol. 79, pp. 464–71, 03 1989.
- [18] J. Su, J. Dai, Z. Guan, Z. SUN, W. Ye, and C. Rajagopalan, "A four-lead real time arrhythmia analysis algorithm," 09 2017.
- [19] Y. Yan, X. Qin, Y. Wu, N. Zhang, J. Fan, and L. Wang, "A restricted boltzmann machine based two-lead electrocardiography classification," in *2015 IEEE 12th International Conference on Wearable and Implantable Body Sensor Networks (BSN)*, June 2015, pp. 1–9.
- [20] P. Chazal, "Different techniques used to improve the performance of a classifier of the twelve-lead electrocardiogram," 02 2001, pp. 525 – 528.
- [21] F.-W. La and P.-Y. Tsai, "Deep learning for detection of fetal ecg from multi-channel abdominal leads," 11 2018, pp. 1397–1401.
- [22] E. Luz, W. Schwartz, G. Chvez, and D. Menotti, "Ecg-based heartbeat classification for arrhythmia detection: A survey," *Computer Methods and Programs in Biomedicine*, vol. 127, 12 2015.
- [23] C. Ye, B. V. K. V. Kumar, and M. T. Coimbra, "An automatic subject-adaptable heartbeat classifier based on multiview learning," *IEEE Journal of Biomedical and Health Informatics*, vol. 20, no. 6, pp. 1485–1492, Nov 2016.
- [24] T. Ince*, S. Kiranyaz, and M. Gabbouj, "A generic and robust system for automated patient-specific classification of ecg signals," *IEEE Transactions on Biomedical Engineering*, vol. 56, no. 5, pp. 1415–1426, May 2009.
- [25] W. Jiang and S. G. Kong, "Block-based neural networks for personalized ecg signal classification," *IEEE Transactions on Neural Networks*, vol. 18, no. 6, pp. 1750–1761, Nov 2007.
- [26] Y. H. Hu, S. Palreddy, and W. J. Tompkins, "A patient-adaptable ecg beat classifier using a mixture of experts approach," *IEEE Transactions on Biomedical Engineering*, vol. 44, no. 9, pp. 891–900, Sep. 1997.
- [27] "Recommended practice for testing and reporting performance results of ventricular arrhythmia detection algorithms," Arlington, VA, USA: Association Advancement Medical Instrumentation, 1987.
- [28] T. Teijeiro, P. Flix, J. Presedo, and D. Castro, "Heartbeat classification using abstract features from the abductive interpretation of the ecg," *IEEE Journal of Biomedical and Health Informatics*, vol. 22, no. 2, pp. 409–420, March 2018.
- [29] G. B. Moody and R. G. Mark, "The impact of the mit-bih arrhythmia database," *IEEE Engineering in Medicine and Biology Magazine*, vol. 20, no. 3, pp. 45–50, May 2001.
- [30] A. Goldberger, L. Amaral *et al.*, "Physiobank, physiotoolkit, and physionet : Components of a new research resource for complex physiologic signals," *Circulation*, vol. 101, pp. E215–20, 07 2000.
- [31] P. Sabherwal, M. Aggarwal, and L. Singh, "Automatic detection of the r peaks in single-lead ecg signal," *Circuits Systems and Signal Processing*, vol. 36, 03 2017.
- [32] J. Pan and W. J. Tompkins, "A real-time qrs detection algorithm," *IEEE Transactions on Biomedical Engineering*, vol. BME-32, no. 3, pp. 230–236, March 1985.
- [33] C. Li, C. Zheng, and C. Tai, "Detection of ecg characteristic points using wavelet transforms," *IEEE transactions on bio-medical engineering*, vol. 42, no. 1, p. 2128, January 1995.
- [34] C. Ye, B. V. K. Vijaya Kumar, and M. T. Coimbra, "Heartbeat classification using morphological and dynamic features of ecg signals," *IEEE Transactions on Biomedical Engineering*, vol. 59, no. 10, pp. 2930–2941, Oct 2012.
- [35] S. Yang, "Several tips and tricks for imagenet cnn training," *Technique Report*, pages 1-12, 2016.
- [36] K. W. Bowyer, N. V. Chawla, L. O. Hall, and W. P. Kegelmeyer, "SMOTE: synthetic minority over-sampling technique," *CoRR*, vol. abs/1106.1813, 2011. [Online]. Available: <http://arxiv.org/abs/1106.1813>
- [37] G. E. A. P. A. Batista, A. L. C. Bazzan, and M. C. Monard, "Balancing training data for automated annotation of keywords: a case study," in *II Brazilian Workshop on Bioinformatics, December 3-5, 2003, Macaé, RJ, Brazil*, 2003, pp. 10–18.
- [38] K. He, X. Zhang, S. Ren, and J. Sun, "Identity mappings in deep residual networks," *CoRR*, vol. abs/1603.05027, 2016.
- [39] J. Hu, L. Shen, and G. Sun, "Squeeze-and-excitation networks," *CoRR*, vol. abs/1709.01507, 2017.
- [40] J. Wang, "Proposed new requirements for testing and reporting performance results of arrhythmia detection algorithms," *Journal of Electrocardiology*, vol. 47, 12 2014.
- [41] R. Shwartz-Ziv and N. Tishby, "Opening the black box of deep neural networks via information," *CoRR*, vol. abs/1703.00810, 2017.
- [42] N. Tishby and N. Zaslavsky, "Deep learning and the information bottleneck principle," *2015 IEEE Information Theory Workshop, ITW 2015*, 03 2015.